ELSEVIER

International Journal of Mass Spectrometry 194 (2000) 93–101

International Journal of Mass Spectrometry

Multiply hydrogen bonded complexes in ether systems: combining experiments with density functional theory calculations

Chuanbao Zhu, Yun Ling[1], Wan Yong Feng[2], Chava Lifshitz[3,*]

Department of Physical Chemistry and The Farkas Center for Light Induced Processes, The Hebrew University of Jerusalem, Givat-Ram, Jerusalem 91904, Israel

Received 15 February 1999; accepted 5 April 1999

Abstract

Reactions of proton bound dimers of dimethyl ether (DME), $(CH_3OCH_3)_2H^+$ studied previously are compared with those of proton bound dimers of tetrahydrofuran (THF), $(c\text{-}C_4H_8O)_2H^+$. Experiments were carried out on a selected ion flow tube (SIFT). Base molecules having protic hydrogens such as NH_3, CH_3NH_2, and Me_2NH, which are capable of forming multiply hydrogen bonded core ions, undergo insertion into the THF dimer but not into the DME dimer. The potential energy profiles for the association-insertion reactions of ammonia with both dimers were calculated using the density functional theory (DFT) at the B3LYP/cc-pVTZ level of theory. The insertion of ammonia into $(DME)_2H^+$ or $(THF)_2H^+$ demonstrates high central barriers in double-well potential energy profiles. RRKM/QET rate constant calculations on the two surfaces give results which are in agreement with the experimental branching ratios between the reaction channels of insertion and switching. (Int J Mass Spectrom 194 (2000) 93–101) © 2000 Elsevier Science B.V.

Keywords: Proton bound clusters; SIFT; DFT; RRKM; Ion complexes

1. Introduction

Multiply hydrogen bonded complexes are of great importance in chemical and biological systems. We have discovered in recent years [1] a unique insertion reaction of base molecules having protic hydrogens such as NH_3, CH_3NH_2, Me_2NH, and CH_3OH. These molecules insert into proton bound, alkyl blocked dimers, for example, $(CH_3CN)_2H^+$ and $(CH_3COCH_3)_2H^+$, by virtue of their ability to form multiply hydrogen bonded core ions. They undergo a similar insertion reaction into the protonated 12-crown-4 ether [2]. The insertion complexes are collisionally stabilized. The reaction of acetonitrile dimer and ammonia is shown schematically below with helium as the stabilizing third-body:

$$(CH_3CN)_2H^+ + NH_3 \xrightarrow{He} (CH_3CN)_2NH_4^+ \qquad (1)$$

The mechanisms of insertion of amines and alcohols into proton bound acetonitrile and acetone dimers, on the one hand, and into 12-crown-4 ether and

* Corresponding author.

[1] Present address: Department of Chemistry, York University, Toronto, Ontario, Canada M3J 1P3.

[2] Present address: Department of Chemistry and Biochemistry, San Francisco State University, 1600 Holloway Avenue, CA 94132.

[3] Archie and Marjorie Sherman Professor of Chemistry.

Dedicated to Professor Jim Morrison on the occasion of his 75th birthday.

PII S1387-3806(99)00123-2

dimethoxyethane, on the other, were investigated recently by density functional theory (DFT) calculations [3,4]. Some salient structures along the reaction coordinate for insertion of NH_3 into the protonated acetonitrile dimer were deduced [3].

Double-well potential energy profiles with a central barrier have proved to be useful in understanding the reaction efficiencies of ion/molecule reactions [5]. Alkyl blocked protonated dimers are characterized by ion/molecule reactions having low efficiencies [1]. It was assumed that these reactions proceed via double-well potential surfaces with intermediate barriers [1] in which the first step is due to the formation of a relatively loose ion-dipole complex. In the case of reaction with ammonia, e.g., reaction (1), the second well is due to a more strongly bound complex of the ammonium ion forming two hydrogen bonds with each of the original monomer acetonitrile molecules making up the original dimer. Symmetrical triple-well potential energy surfaces are important in the H/D exchange of protonated glycine oligomers with ND_3 [6]. The first well is due to formation of an ion-dipole complex. The third well is for the deuterium exchanged ion/dipole complex and is of similar depth as the first well. The central well is deeper and is due to endothermic proton transfer to ammonia, which is rendered energetically feasible by simultaneous solvation of the resultant ammonium ion by hydrogen bonding to the neutral peptide. This multistep insertion mechanism is thus important not only in protonated cluster systems but also for biologically important molecules such as peptides and proteins.

We have found already in our first investigation [1] that the ether family of molecules is unique. Unlike other alkyl blocked dimers, the proton bound dimer of dimethyl ether (DME) does not undergo an association-insertion reaction with ammonia, methylamine and dimethylamine. It was suggested that the lack of association-insertion in the case of $(CH_3OCH_3)_2H^+$ is due to steric hindrance. Because insertion into the proton bound dimer of tetrahydrofuran (THF), $(c\text{-}C_4H_8O)_2H^+$ was observed [1] it was thought that steric hindrance is lifted in the case of THF.

The purpose of the present research has been to study the reactivity of $(THF)_2H^+$ and $(DME)_2H^+$ experimentally by the selected ion flow tube (SIFT) technique and computationally by density functional theory (DFT) calculations. The potential energy profiles for the reactions of both dimers with ammonia were calculated comparatively at the same theoretical levels of B3LYP/cc-pVDZ and B3LYP/cc-pVTZ. It will be shown that both reactions are characterized by similarly high central barriers. The different behavior of the two reactions reflects competition between unimolecular dissociation of the insertion complex and collisional stabilization of the complex. This competition depends on the number of degrees of freedom and can be reproduced by RRKM calculations.

2. Methods

2.1. Experimental section

The SIFT apparatus employed has been described in detail [7]. Briefly, reactant ions are generated in a suitable ion source, mass-selected by a quadrupole mass filter, and injected into the flow tube by a helium carrier gas via a Venturi inlet. A neutral reactant is introduced into the flow tube at an appropriate distance downstream to ensure laminar flow. A detector quadrupole filter analyzes the reactant and product ions.

We were unable to inject the protonated dimers from the ion source into the flow tube. We injected the protonated monomers, $(DME)H^+$ and $(THF)H^+$, which were converted fully as before [1] into the corresponding dimers, by the collision-stabilized association reactions [8–10],

$$AH^+ + A + He \rightarrow A_2H^+ + He \quad (2)$$

where A is DME or THF, respectively. Optimal flow rates were 1.5 to 2 standard $cm^3\ min^{-1}$ for reactant A and 7 standard L min^{-1} for He. The helium pressure in the tube was 0.32 Torr and the temperature was 300 K. The effective second order dimerization rate constant [for reaction (2)] was determined to be 5.4×10^{-10} cc/molecule s in the case of THF.

Second-order rate coefficients were obtained by

monitoring the intensity of the primary A_2H^+ ion decay as a function of the neutral reactant gas B concentration introduced downstream from the inlet of A. Experimental reproducibilities for rate constant measurements were ~±22%. Product ion distributions were obtained by plotting the percentage of each product ion as a function of the gas B flow rate and extrapolating the resulting curves to zero flow rate. Product ion distributions were corrected via the measured mass discrimination factors of the detector quadrupole mass filter.

2.2. Computational

All DFT calculations have been carried out using the Gaussian 94 package [11] running on a DEC Alpha TurboLaser 8400 at the Institute of Chemistry, Hebrew University. These calculations employed the B3LYP (Becke three-parameter Lee-Yang-Parr) exchange-correlation functional [12,13], which combines the Becke three-parameter exchange functional [12] with the gradient-corrected correlation functional of Lee et al. [13]. Apart from the standard 4-31G basis set, the basis sets employed belong to the correlation consistent [14,15] family of Dunning and co-workers. The cc-pVDZ (correlation consistent polarized valence double ζ) basis set is a [3s2p1d/2s1p] contraction of a (9s4p1d/4s1p) basis set. The cc-pVTZ (correlation consistent polarized valence triple ζ) set is a [4s3p2d1f/3s2p1d] contraction of a (10s5p2d1f/5s2p1d) basis set. The aug-cc-pVTZ (augmented cc-pVTZ) set additionally carries one low-exponent basis function of each angular momentum to accommodate anions, highly polar molecules, and weak molecular interactions. The geometry of each species was completely optimized at the B3LYP/4-31G level. These calculations were then extended to the cc-pVDZ basis set. Vibrational frequencies were computed for all optimized geometries. Finally, single point energies were also calculated for the optimized geometries at the basis set level of cc-pVTZ.

RRKM/QET calculations were carried out on the ab initio potential energy surfaces using scaled vibrational frequencies from the DFT calculations. C-H stretching vibrations were scaled by a factor of 0.96 while all other frequencies were scaled by a factor of 0.976.

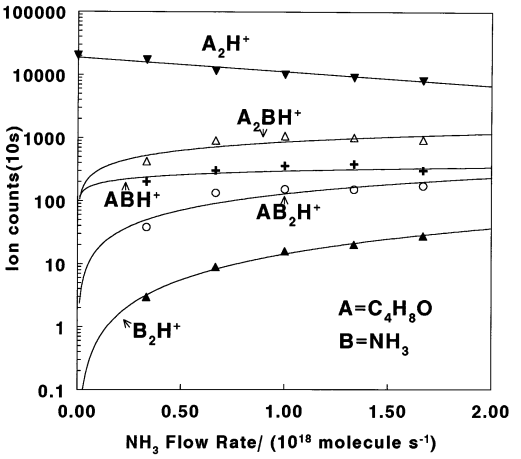

Fig. 1. Variation of primary and product ion count rates with ammonia flow rate for the reaction of protonated tetrahydrofuran (THF) dimer, with ammonia, B. A_2H^+, proton bound THF dimer: line and filled triangle; A_2BH^+, insertion complex of ammonia into the protonated dimer: open triangle △; ABH^+, protonated mixed dimer of THF and ammonia: cross +; AB_2H^+, protonated trimer of THF and two ammonias: open circle; B_2H^+, protonated ammonia dimer: filled triangle.

3. Results and discussion

3.1. Experimental

By analogy with reactions observed previously for other alkyl blocked dimers [1], the proton bound dimer of THF undergoes three typical reactions: insertion (IN, called earlier [1] association, AS), switching (SW), and proton transfer (PT). We shall concentrate here on those reaction partners which demonstrate the association-insertion channel, IN. A plot for reactant and product ion counts as a function of the neutral base flow rate is shown in Fig. 1 for the reaction of $(THF)_2H^+$ with ammonia. Figs. 2 and 3 show plots for product ion branching ratios for $(THF)_2H^+$ with methylamine and with dimethylamine, respectively, as a function of the neutral flow rates. The insertion and switching channels, A_2BH^+ and ABH^+, are primary reactions in all cases while

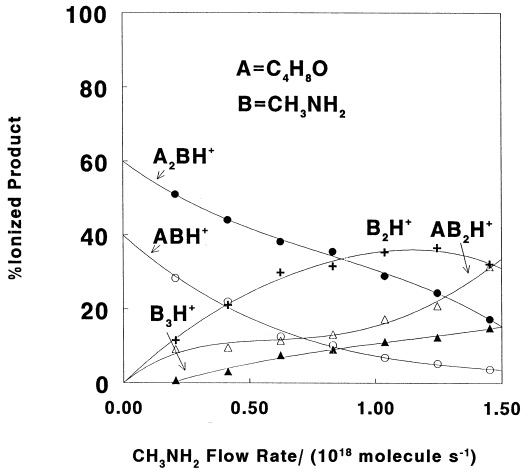

Fig. 2. Product ion distribution as a function of methylamine flow rate for the reaction of protonated THF dimer with methylamine, B. A_2BH^+, insertion complex: filled circle; ABH^+, switching product, open circle; B_2H^+, protonated methylamine dimer: cross; B_3H^+, protonated methylamine trimer: filled triangle; AB_2H^+, protonated trimer of THF and two methylamines: open triangle.

AB_2H^+, B_2H^+ and B_3H^+ are secondary reaction channels. Proton transfer to form BH^+ is a very minor primary channel for dimethylamine (Fig. 3). Reaction efficiencies, r_{eff} have been calculated by dividing the

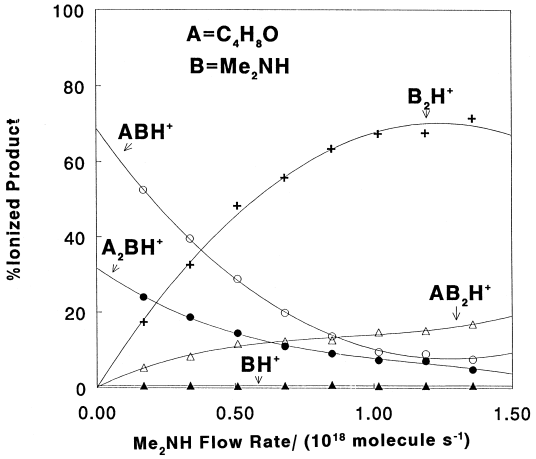

Fig. 3. Product ion distribution as a function of dimethylamine flow rate for the reaction of protonated THF dimer with dimethylamine, B. A_2BH^+, insertion complex: filled circle; ABH^+, switching product, open circle; BH^+, protonated dimethylamine: filled triangle; B_2H^+, protonated dimethylamine dimer: cross; AB_2H^+, protonated trimer of THF and two dimethylamines: open triangle.

effective second order experimental rate constants by the corresponding collision rate constants. The latter were calculated by using the parametrized expression of Su and Chesnavich [16]. Reaction efficiencies and product branching ratios for reactions of $(DME)_2H^+$ (from [1]) and for reactions of $(THF)_2H^+$ (present results) are summarized in Table 1. The reaction efficiencies for the protonated THF dimer are lower than for the corresponding DME dimer. On the other hand, the base molecules studied, namely ammonia, methyl amine and dimethylamine, undergo insertion into $(THF)_2H^+$ and the collisionally stabilized trimers are observed, whereas insertion products are not observed for $(DME)_2H^+$.

3.2. Computations

Extension of the basis set from 4-31G to cc-pVDZ was found to lower the energy of each of the species studied to a considerable degree, whereas this extension has hardly any effect on the geometries. All the relevant geometries for the insertion reactions of ammonia into the protonated dimers of DME and THF, optimized at the B3LYP/cc-pVDZ level of theory, are presented in Figs. 4 and 5, respectively. The energies calculated were found to be more sensitive to the basis sets employed as expected. This sensitivity was tested on the DME/ammonia and THF/ammonia insertion complexes whose geometries were optimized at the B3LYP/cc-pVDZ level. The calculated single point energies for different basis sets according to Dunning and coworkers [14,15], as well as for the 6-311++G(2d, p) basis set are presented in Table 2, as are the energy differences relative to the B3LYP/cc-pVDZ calculation. These comparative calculations lead us to the conclusion that the energies for all species of interest in this study need to be calculated at least with the cc-pVTZ basis set, but that extension to the aug-cc-pVTZ set is not necessary because there are only minor differences between the cc-pVTZ and aug-cc-pVTZ results. The remaining differences disappear totally when relative energies are calculated for the potential energy profiles. The resultant energies for all the species of interest are summarized in Table 3.

Table 1
Reaction efficiencies and product branching ratios for reactions of $(DME)_2H^+$ and $(THF)_2H^+$ with a series of base molecules, B.

	$(DME)_2H^+$				$(THF)_2H^+$			
		Product ion distribution (%)				Product ion distribution (%)		
B	r_{eff}	IN	SW	PT	r_{eff}	IN	SW	PT
1. NH_3	0.067	···	99.9	0.1	0.015	64	36	···
2. $MeNH_2$	0.18	···	98	2	0.06	60	40	···
3. $(Me)_2NH$	0.13	···	94	6	0.06	31.5	68	0.5

The insertion mechanism into the DME and THF dimers, respectively, has been investigated using an intrinsic reaction coordinate (IRC) calculation [17,18] as has been done previously [3] in the case of acetonitrile. This analysis verified that the transition state found belongs indeed to the reaction coordinate of interest, namely the insertion of ammonia into the protonated dimer of DME or THF.

The potential energy profiles for the insertion reactions of ammonia into $(DME)_2H^+$ and $(THF)_2H^+$ were calculated at the B3LYP/cc-pVTZ//B3LYP-/cc-pVDZ level. The energies relative to the entrance

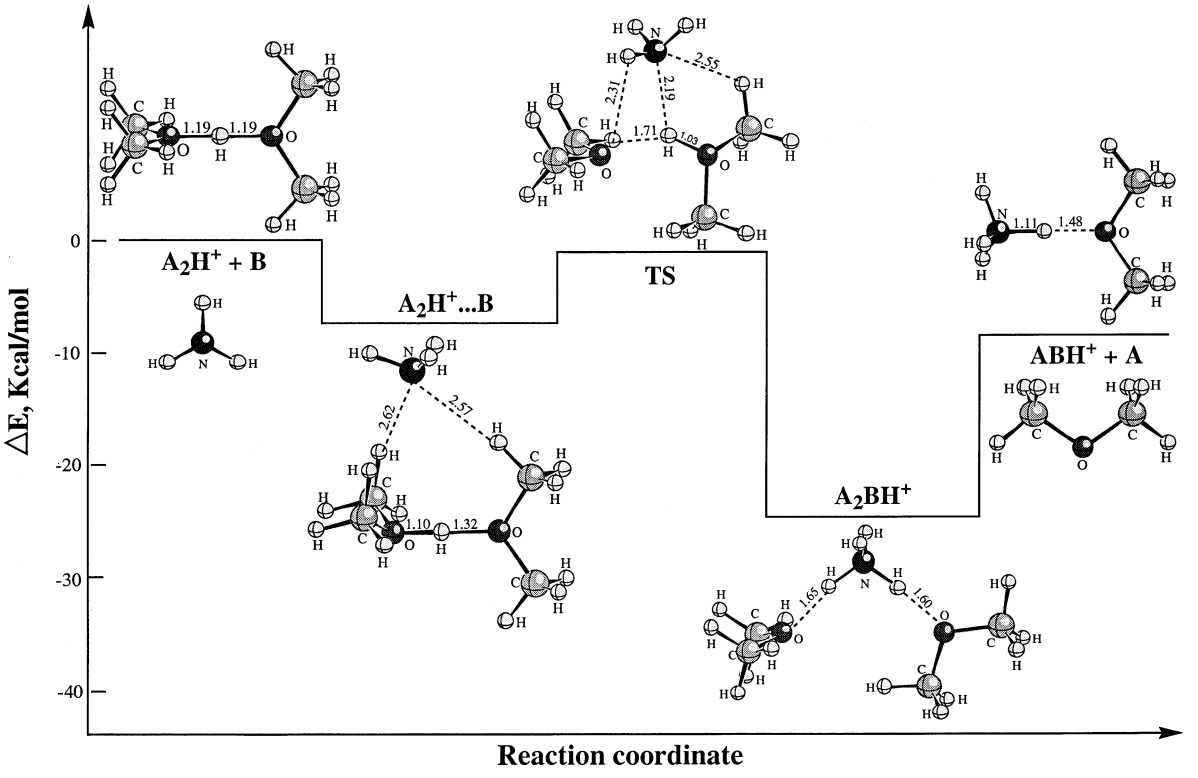

Fig. 4. B3LYP/cc-pVDZ computed relevant structures and potential energy profile along the reaction coordinate for insertion of ammonia, B into the proton bound dimer of DME, A_2H^+; A_2H^+ . . . B: ion-dipole complex; A_2BH^+: insertion complex; TS: transition state. The structures include hydrogen bond distances (Å); the energies were calculated at the B3LYP/cc-pVTZ//B3LYP/cc-pVDZ level and include zero point energies.

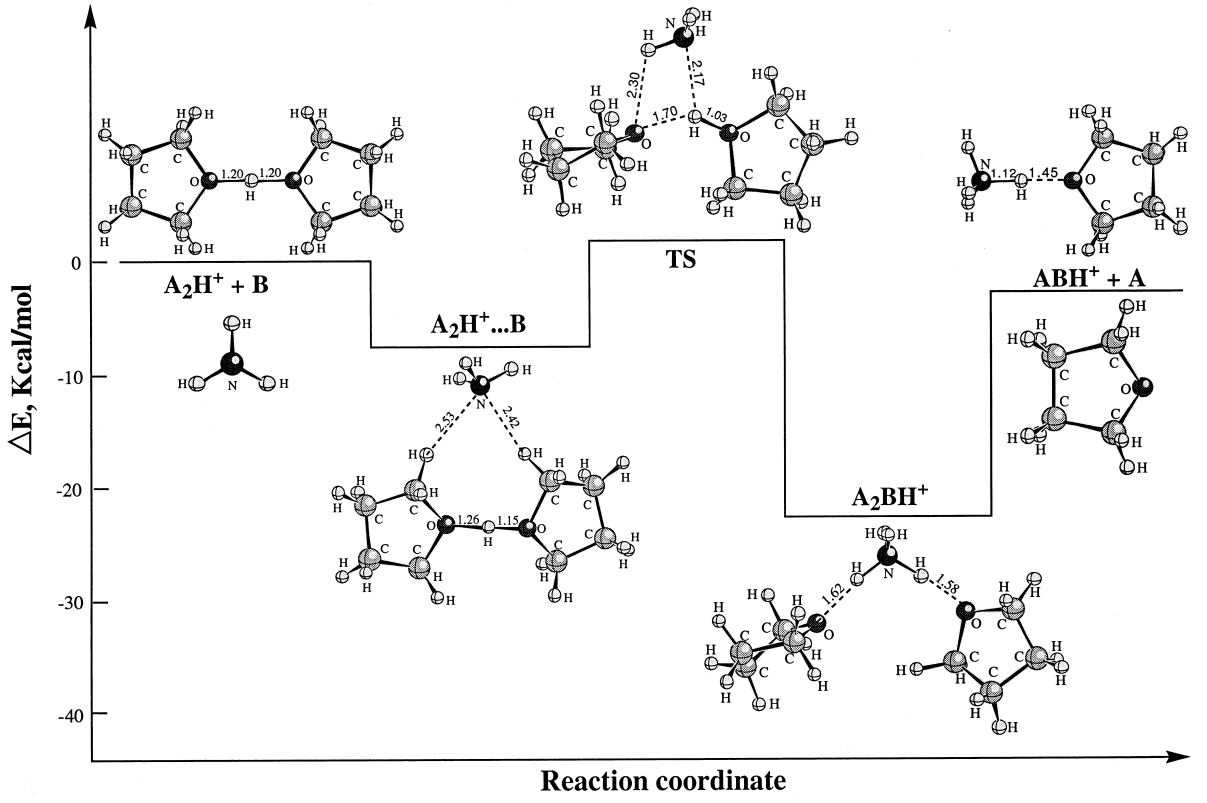

Fig. 5. B3LYP/cc-pVDZ computed relevant structures and potential energy profile along the reaction coordinate for insertion of ammonia, B into the proton bound dimer of THF, A_2H^+; $A_2H^+ \ldots B$: ion-dipole complex; A_2BH^+: insertion complex; TS: transition state. The structures include hydrogen bond distances (Å); the energies were calculated at the B3LYP/cc-pVTZ//B3LYP/cc-pVDZ level and include zero point energies.

channels taken as zero, including zero point energies, are summarized in Table 4 and the profiles themselves are included in Figs. 4 and 5, respectively. The reactions are characterized by double-well potential profiles. The first, more shallow well belongs to the ion/dipole complex, whereas the second deeper well is that of the insertion complex. There are high central barriers in both surfaces.

Table 2
Energies of the insertion complexes for various basis sets with B3LYP

	DME		THF	
Basis set[a]	Energy (hartree)	Energy difference[b] (kcal/mol)	Energy (hartree)	Energy difference[b] (kcal/mol)
pVDZ	−367.032 620 1	0	−521.898 518 9	0
AVDZ//pVDZ	−367.063 861 4	−19.6	−521.938 860 8	−25.31
pVTZ//pVDZ	−367.171 037 7	−86.9	−522.076 111 6	−111.44
AVTZ//pVDZ	−367.175 102 9	−89.4	−522.081 028 3	−114.53
6-311++G(2d, p) //pVDZ	−367.146 478 8	−71.5	−522.042 959 4	−90.64

[a] pVDZ = cc-pVDZ, pVTZ = cc-pVTZ, AVDZ = aug-cc-pVDZ, AVTZ = aug-cc-pVTZ.
[b] Relative to the energy at B3LYP/cc-pVDZ.

Table 3
Overview of stationary points for species relevant to the reactions of $(CH_3OCH_3)_2H^+$ and $(c\text{-}C_4H_8O)_2H^+$ with NH_3

Species	E(B3LYP/cc-pVDZ) (hartree)	ZPE (kcal/mol)	E(B3LYP/cc-pVTZ//B3LYP/cc-pVDZ) (hartree)
NH_3	−56.554 254 8	21.38	−56.584 330 8
NH_4^+	−56.899 711 6	30.72	−56.925 094 4
CH_3OCH_3	−155.029 424 7	49.52	−155.089 323 3
$(CH_3)_2OH^+$	−155.344 370 4	57.86	−155.403 632 3
$(CH_3)_2O \ldots NH_4^+$	−211.970 914 8	81.01	−212.053 215 9
$(CH_3)_2O \ldots H^+ \ldots O(CH_3)_2$[a]	−310.425 371 1	106.47	−310.540 815 4
$(CH_3OCH_3)_2H^+ \ldots NH_3$[b]	−367.000 697 4	130.61	−367.140 794 7
$(CH_3)_2O \ldots NH_4^+ \ldots O(CH_3)_2$[c]	−367.032 620 1	132.30	−367.171 037 7
insertion transition state (DME)	−366.991 720 1	131.10	−367.131 267 9
$c\text{-}C_4H_8O$	−232.457 721 6	72.82	−232.537 200 4
$(c\text{-}C_4H_8O)H^+$	−232.787 099 8	80.80	−232.866 340 2
$(c\text{-}C_4H_8O)NH_4^+$	−289.405 965 8	103.92	−289.507 419 5
$(c\text{-}C_4H_8O)_2H^+$	−465.295 981 5	152.30	−465.450 241 9
$(c\text{-}C_4H_8O)_2H^+ \ldots NH_3$	−521.869 648 1	176.00	−522.049 448 6
$(c\text{-}C_4H_8O)_2NH_4^+$	−521.898 518 9	178.42	−522.076 111 6
insertion transition state (THF)	−521.861 012 7	177.05	−522.037 173 4

[a] Proton-bound dimer.
[b] Ion-dipole complex.
[c] Insertion complex.

Each of the two insertion reactions progresses along the following steps:

$$A_2H^+ + NH_3 \underset{k_1}{\overset{k_c}{\rightleftharpoons}} A_2H^+ \cdots NH_3 \underset{k_3}{\overset{k_2}{\rightleftharpoons}}$$

$$[A \cdots \underset{\downarrow k_5}{NH_4^+} \cdots A] \xrightarrow{k_4} A \cdots NH_4^+ + A \qquad (3)$$
$$A_2NH_4^+$$

The reaction efficiency, r_{eff} is given by

$$r_{eff} = \frac{k_2}{k_1 + k_2} \qquad (4)$$

Reaction (1) proceeds via a loose, orbiting transition state (OTS). We have calculated the activation entropy for going from the ion dipole complex to the central barrier using the scaled DFT vibrational frequencies and found it to be $\Delta S^{\#} = -5$ eu, indicating a tight transition state (TTS) for reaction (2), as expected. The r_{eff} calculated is very sensitive to $\Delta E^{\#}$ [20], where

$$\Delta E^{\#} = E_{reactants} - E_{barrier} \qquad (5)$$

however, the barrier energy is the least reliable of the values calculated by ab initio DFT and $\Delta E^{\#}$ is a small difference between two large numbers. As $\Delta E^{\#} \rightarrow 0$, $r_{eff} \rightarrow 0$, provided that the reactants have no excess energy. Both the DME and the THF reactions with

Table 4
Relative energies (kcal/mol) at the B3LYP/cc-pVTZ//B3LYP/cc-pVDZ level for the reaction profiles of $(CH_3OCH_3)_2H^+$ and $(c\text{-}C_4H_8O)_2H^+$, respectively, with NH_3

Species	ΔE[a]
$(CH_3OCH_3)_2H^+ + NH_3$[b]	0
$(CH_3OCH_3)_2H^+ \ldots NH_3$(I)	−7.05
TS between (I) and (II)	−0.58
$(CH_3)_2O \ldots NH_4^+ \ldots O(CH_3)_2$(II)	−24.04
$(CH_3)_2O \ldots NH_4^+ + CH_3OCH_3$[b]	−8.26
$(c\text{-}C_4H_8O)_2H^+ + NH_3$[b]	0
$(c\text{-}C_4H_8O)_2H^+ \ldots NH_3$(III)	−7.02
TS between (III) and (IV)	+1.84
$(c\text{-}C_4H_8O) \ldots NH_4^+ \ldots (c\text{-}C_4H_8O)$(IV)	−21.33
$c\text{-}C_4H_8ONH_4^+ + c\text{-}C_4H_8O$[b]	−3.25

[a] With 0.976 [19] scaled ZPE correction.
[b] With size-consistence correction.

ammonia demonstrate low efficiencies (Table 1)—6.7% and 1.5%, respectively—and the central barriers are indeed very high for both. The calculated values are $\Delta E^{\#} = 0.58$ kcal/mol and -1.84 kcal/mol for DME and THF, respectively. The central barrier for insertion into $(THF)_2H^+$ is higher than for $(DME)_2H^+$ in agreement with the lower overall reaction efficiency of the THF reaction. The calculated $\Delta E^{\#}$ value for the THF reaction is negative; however, high level calculations might make this difference positive. It is also possible that the reaction is observed in spite of a negative $\Delta E^{\#}$ value because of the tail of the thermal energy distribution of the reactants at room temperature. When comparing RRKM calculations carried out on ab initio surfaces with experimental results, the activation barrier has very often been treated as a parameter because of the errors associated with ab initio calculations of transition state energies [21,22]. It is possible to treat $\Delta E^{\#}$ as a parameter and to calculate k_1 and k_2 until one gets a fit with the experimental reaction efficiency [20]. This has not been done in the present case because the uncertainties in the calculations were considered to be too large.

The branching ratio between the switching and insertion channels, SW/IN, (Table 1) is equal to k_4/k_5 and is calculable. The pseudo-first-order deactivation rate constant k_5 is given by

$$k_5 = k'_c \times \beta \times [\mathrm{He}], \quad (6)$$

where k'_c is the collision rate with helium, [He] is the helium concentration, and β is the collisional deactivation efficiency of helium. If $\beta \cong 0.1$, then $k_5 \cong 5 \times 10^5\ s^{-1}$, for both reaction systems. However, k_4 is three orders of magnitude higher for the DME reaction than for the THF reaction. For a relatively loose transition state with $\Delta S^{\#} = +3$ eu, $k_4 = 1 \times 10^8\ s^{-1}$ for DME leading to a branching ratio between switching and insertion in excess of 200:1, which explains why no insertion of ammonia into the protonated DME dimer is observed under our experimental conditions. On the other hand, $k_4 = 1.1 \times 10^5\ s^{-1}$ in the case of THF, for a transition state of similar degree of looseness, leading to a calculated branching ratio of switching versus insertion of 0.22:1, which is very near the experimental ratio of 0.56:1 found for THF (0.36:0.64; Table 1). The experimental ratio between switching and insertion observed for the ammonia/THF reaction corresponds to a value of $k_4 = 2.8 \times 10^5\ s^{-1}$, which is only slightly higher than calculated.

4. Conclusions

Combining experimental SIFT results with DFT and RRKM calculations has been very useful in demonstrating that ammonia does insert into the proton bound dimer of DME but that the insertion complex is too short lived to be stabilized at the pressures prevailing in the flow tube and breaks up into the proton bound mixed DME/ammonia dimer and free DME. On the other hand, the insertion complex can be stabilized by collisions with helium in the case of THF. The present conclusion has to be that the differences between insertion reactions into the protonated dimers of DME and THF are not related to differences in steric hindrance contrary to previous conclusions [1]. There are obviously remaining unanswered questions; for example, the fact that insertion into the acetonitrile dimer is observed experimentally although the potential energy profiles of DME and acetonitrile are quite similar as are the numbers of degrees of freedom involved in these two systems. Further work along similar lines is thus warranted.

Acknowledgements

This research was supported by the Israel Science Foundation founded by the Israel Academy of Sciences and Humanities. The Farkas Research Center is supported by the Minerva Gesellschaft für die Forschung GmbH, München.

Chava Lifshitz thanks Jim Morrison who had a profound influence on her in her early stages of scientific development while she was a postdoctoral fellow at Cornell University and he came for a visit.

References

[1] W.Y. Feng, M. Goldenberg, C. Lifshitz, J. Am. Soc. Mass Spectrom. 5 (1994) 695.
[2] W.Y. Feng, C. Lifshitz, J. Am. Chem. Soc. 117 (1995) 11548.
[3] J.M.L. Martin, V. Aviyente, C. Lifshitz, J. Phys. Chem. A 101 (1997) 2597.
[4] D. Adötoledo, V. Aviyente, J.M.L. Martin, C. Lifshitz, J. Phys. Chem. A 102 (1998) 6357.
[5] W.N. Olmstead, J.I. Brauman, J. Mass Spectrom. 30 (1995) 1649.
[6] S. Campbell, M.T. Rodgers, E.M. Marzluff, J.L. Beauchamp, J. Am. Chem. Soc. 117 (1995) 12840.
[7] M. Iraqi, A. Petrank, M. Peres, C. Lifshitz, Int. J. Mass Spectrom. Ion Proc. 100 (1990) 679.
[8] M.J. McEwan, A.B. Denison, V.G. Anicich, W.T. Huntress Jr., Int. J. Mass Spectrom. Ion Proc. 81 (1987) 247.
[9] P. Kofel, T.B. McMahon, J. Phys. Chem. 92 (1988) 6174.
[10] V.G. Anicich, A.D. Sen, W.T. Huntress, M.J. McEwan, J. Chem. Phys. 94 (1991) 4189.
[11] M.J. Frisch, G.W. Trucks, H.B. Schlegel, P.M.W. Gill, B.G. Johnson, M.A. Robb, J.R. Cheeseman, T. Keith, G.A. Petersson, J.A. Montgomery, K. Raghavachari, M.A. Al-Laham, V.G. Zakrzewski, J.V. Ortiz, J.B. Foresman, J. Cioslowski, B.B. Stefanov, A. Nanayakkara, M. Challacombe, C.Y. Peng, P.Y. Ayala, W. Chen, M.W. Wong, J.L. Andres, E.S. Replogle, R. Gomperts, R.L. Martin, D.J. Fox, J.S. Binkley, D.J. Defrees, J. Baker, J.P. Stewart, M. Head-Gordon, C. Gonzalez, J.A. Pople, GAUSSIAN 94, Revision E.2; Gaussian, Inc.: Pittsburgh, 1995.
[12] A.D. Becke, J. Chem. Phys. 98 (1993) 5648.
[13] C. Lee, W. Yang, R.G. Parr, Phys. Rev. B 37 (1988) 785.
[14] T.H. Dunning Jr., J. Chem. Phys. 90 (1989) 1007.
[15] R.A. Kendall, T.H. Dunning Jr., R.J. Harrison, J. Chem. Phys. 96 (1992) 6796.
[16] T. Su, W.J. Chesnavich, J. Chem. Phys. 76 (1982) 5182.
[17] K. Fukui, Acc. Chem. Res. 14 (1981) 363.
[18] C. Gonzales, H.B. Schlegel, J. Chem. Phys. 90 (1989) 2154; J. Phys. Chem. 94 (1990) 5523.
[19] J.M.L. Martin, Chem. Phys. Lett. 262 (1996) 97.
[20] P.A.M. van Koppen, J. Brodbelt-Lustig, M.T. Bowers, D.V. Dearden, J.L. Beauchamp, E.R. Fisher, P.B. Armentrout, J. Am. Chem. Soc. 112 (1990) 5663; 113 (1991) 2359.
[21] J.A. Booze, K.-M. Weitzel, T. Baer, J. Chem. Phys. 94 (1991) 3649.
[22] D. Schröder, D. Sülzle, O. Dutuit, T. Baer, H. Schwarz, J. Am. Chem. Soc. 116 (1994) 6395.